NURETH14-403

ANALYSIS OF PSBT BENCHMARK EXERCISES FOR VOID DISTRIBUTION AND DNB USING A SUBCHANNEL CODE MATRA

Dae-Hyun Hwang, Seong Jin Kim, Kyoung-Won Seo Korea Atomic Energy Research Institute, Daejeon, Korea

Abstract

In the framework of OECD/NRC PSBT benchmark, the subchannel grade void distribution data and DNB data were evaluated by a subchannel code MATRA. The zone-averaged void fraction at the central region of the 5x5 test bundle was compared with the benchmark data. Optimum values of turbulent mixing parameter, which is an input parameter for MATRA code, were evaluated by employing subchannel fluid temperature data. The influence of mixing vanes on the subchannel flow distribution was examined through a CFD analysis. The steady-state DNB benchmark data with uniform and non-uniform axial power shapes were evaluated by several DNB prediction models including an empirical correlation, CHF lookup table, and representative mechanistic DNB models with subchannel cross-sectional averaged local properties.

Introduction

The critical heat flux (CHF) is a parameter of great importance which constrains the thermal power capability of a light water nuclear reactor (LWR). It is usually predicted by a local parameter CHF correlation accompanied with an appropriate thermal-hydraulic field analysis code to obtain the subchannel grade local conditions in the fuel assembly. For this purpose, the subchannel approach has been widely adopted in the design calculation of an LWR core since it provides reasonably accurate results on the flow and enthalpy distributions in rod bundles with pertinent computing time.

The OECD/NRC PWR Subchannel and Bundle Tests (PSBT) benchmark was organized on the basis of NUPEC database. The purposes of the benchmark are the encouragement to develop a theoretically-base microscopic approach as well as the comparison of currently available computational approaches. The benchmark consists of two separate phases: void distribution benchmark and DNB benchmark. Subchannel-grade void distribution data was employed for validation of a subchannel analysis code under steady-state and transient conditions. DNB benchmark provided subchannel fluid temperature data which can be used to determine the turbulent mixing parameter for a subchannel code. The steady-state and transient DNB data can be used to evaluate and improve the currently available DNB prediction models in PWR bundles. The NUPEC PWR test facility consists of high pressure and high temperature recirculation loop, a cooling loop, and data recording system [1]. The void fraction was measured by two different methods; A gamma-ray beam CT scanner system was used to determine the distribution of density/void fraction over the subchannel at steady-state flow and to define the subchannel averaged void fraction with an accuracy by ±3%. A multi-beam system was used to measure chordal

The 14th International Topical Meeting on Nuclear Reactor Thermalhydraulics, NURETH-14 Toronto, Ontario, Canada, September 25-30, 2011

averaged subchannel void fraction in rod bundle with accuracies of ±4% and ±5% for steady-state and transient, respectively.

The purpose of this study is to provide analysis results for PSBT benchmark problems for void distribution, subchannel mixing, and DNB, as well as to evaluate the applicability of some mechanistic DNB models to PSBT benchmark data with the aid of subchannel analysis results calculated by the MATRA code.

1. MATRA code models for PSBT benchmark analysis

The MATRA is a subchannel analysis code which adopts mixture transport equations for two-phase flow conditions. The continuity, energy, and axial/lateral momentum equations for an arbitrary subchannel *i* are expressed as follows:

Continuity:

$$A_{i} \frac{\partial \rho_{m,i}}{\partial t} + \frac{\partial \dot{m}_{i}}{\partial z} + \sum_{j} w_{ij} + \sum_{j} w'_{i \leftrightarrow j} = 0$$

$$\tag{1}$$

Energy:

$$A_{i} \frac{\partial}{\partial t} \rho_{m,i} h_{m,i} + \frac{\partial}{\partial z} \left(\dot{m}_{i} \hat{h}_{i} \right) + \sum_{j} w_{ij} \hat{h}^{*} + \sum_{j} w'_{ij} \left(h_{i} - h_{j} \right) = Q$$

$$\tag{2}$$

Axial momentum:

$$\frac{\partial \dot{m}_{i}}{\partial t} + \frac{\partial}{\partial z} \left(\frac{\dot{m}_{i}^{2} v'}{A_{i}} \right) + \sum_{j} w_{ij} u^{*} + f_{T} \sum_{j} w'_{ij} \left(u_{i} - u_{j} \right) = -\overline{A} \frac{\partial P}{\partial z} - F_{z}$$

$$(3)$$

Lateral momentum:

$$\frac{\partial w_{ij}}{\partial t} + \frac{\partial}{\partial z} \left(w_{ij} \overline{u}_i \right) + \frac{1}{l} \sum_i w_{ij} \overline{v}_i = \frac{s_{ij}}{l} \left(P_i - P_j \right) - F_{ij} \tag{4}$$

Major unknowns are the coolant density (ρ), axial flow rate (\dot{m}), cross flow (w_{ij}), pressure (P), and enthalpy (h). The subscript 'm' means the two-phase mixture property and superscript "*" means the donor-channel property. The last term of the left-hand side of the conservation equations (1), (2) and (3) represents the net exchange of a mass, energy, and axial momentum due to a turbulent mixing between subchannel i and its surrounding subchannels. By introducing a turbulent mixing parameter, β , which is defined as a ratio of the lateral fluctuating mass flux to the axial mass flux of the fluid in the subchannel, the turbulent mixing flow rate per unit length from subchannel i to j is expressed as

$$w'_{ij} = \beta \cdot s_{ij} \cdot G_{avg} \tag{5}$$

The turbulent mixing parameter is normally determined from a thermal mixing test at single-phase conditions. Two different models for the inter-channel turbulent mixing phenomenon are available in the MATRA code: the equal-mass-exchange (EM) model and the equal-volume-exchange and void-drift (EVVD) model. The net fluctuating mass velocity from channel i to channel j for the EVVD model is expressed as

$$w'_{i \leftrightarrow j} \equiv w'_{ij} - w'_{ji} = \left(w'_{ij}\right)_{SP} \cdot \theta \cdot \left[\left(\alpha_j - \alpha_i\right) - K_{VD} \frac{\left(G_j - G_i\right)}{G_{avg}}\right], \tag{6}$$

where $(w'_{ij})_{sp}$ is the turbulent mixing flow rate per unit length at single-phase conditions, and θ is a two-phase multiplier for the turbulent mixing rate [2]. Detailed description of the correlation parameters are given in reference [3]. This parameter becomes zero for the EM model. Important models of MATRA code for the analysis of PSBT benchmark are summarized in Table 1.

Table 1 MATRA models for the PSBT test data analysis

Parameters	Values			
Two-phase models				
Field equations	Homogeneous mixture			
Subcooled boiling void fraction	Levy model			
Bulk boiling void fraction	Modified Armand model			
Two-phase friction multiplier	Armand model			
 Subchannel interaction models 				
Crossflow resistance factor	0.5			
Turbulent mixing parameter for single-phase	0.04			
Two-phase turbulent mixing model	EM model			
Hydraulic Resistance Models				
Bundle friction factor	0.184 Re ^{-0.2}			
Spacer grid loss factor (MV/ NMV/ SS)	1.0/ 0.7/ 0.4			

MV: Mixing Vaned, NMV: Non-Mixing Vaned, SS: Simple Support

2. Analysis of Phase-I Benchmark Problems

2.1 Single-channel void distribution benchmark

Single subchannel void distribution benchmark provides cross-sectional averaged void fraction at the exit of four different subchannel types found in a PWR assembly: central typical, central thimble, side, and corner subchannel types. The single channel void fraction data was used for the evaluation of void fraction correlations in the subchannel code MATRA. The boiling models described in Table 1 revealed slightly over-prediction of channel exit void fraction for central typical and side subchannels as shown in Figure 1. The mean error and standard deviation of the predicted void fraction(P) minus measured void fraction(M) for the benchmark test series S1 through S4 were calculated by 0.02 and 0.06, respectively.

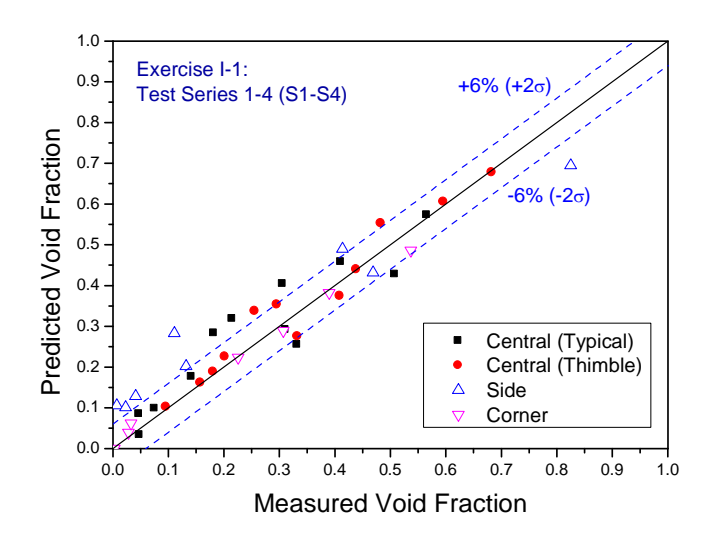


Figure 1 Single-channel void fraction calculated by MATRA code

2.2 Steady-state bundle void distribution benchmark

The benchmark data provided steady-state void fraction averaged over the four central subchannels (CNTR) as shown in Figure 2. The experimental data include chordal averaged void fraction at three axial elevations. Geometry information for the test bundles are summarized in Table 2. The predicted void fractions at three axial levels are compared with corresponding measured data as shown in Figure 3. As the axial elevation increases, the mean error of (P-M) decreases from 0.049 to -0.035 while the standard deviation remains within 0.06 to 0.069 for all axial levels. The maximum error of (P-M) was calculated by 0.11 at the lower elevation of B7 which has central unheated rod and cosine axial power shape. The mean error and standard deviation for all axial levels of test bundles were calculated by 0.014 and 0.073, respectively.

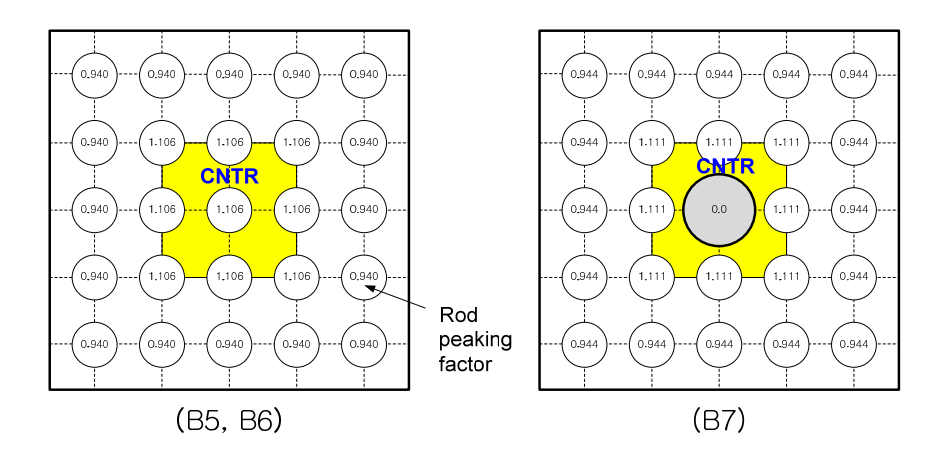


Figure 2 Cross-sectional view of PSBT 5x5 test bundles for Phase-I

Item	Data							
Assembly	B5,B6	В7	A0	A1	A2	A3	A4,A11,A13	A8,A12
Test	Void	Void	DNB	Mixing	DNB	DNB	DNB	DNB
Rod array	5x5	5x5	5x5	5x5	5x5	6x6	5x5	5x5
Number of heated rods	25	24	25	25	25	36	25	24
Number of thimble rods	0	1	0	0	0	0	0	1
Heated rod O.D.	9.50	9.50	9.50	9.50	9.50	9.50	9.50	9.50
Thimble rod O.D.	-	12.24	-	-	-	-	-	12.24
Heated rod pitch	12.60	12.60	12.60	12.60	12.60	12.60	12.60	12.60
Axial heated length	3658	3658	3658	3658	3658	3658	3658	3658
Flow channel inner width	64.9	64.9	64.9	64.9	64.9	77.5	64.9	64.9
Axial power shape	Uni/Cos	Cos	Uni	Uni	Uni	Uni	Cos	Cos
Number of MV spacers	7	7	5	7	7	7	7	7
Number of NMV spacers	2	2	2	2	2	2	2	2
Number of simple spacers	8	8	6	8	8	8	8	8

Table 2 Geometry of test bundles

Length: [mm]

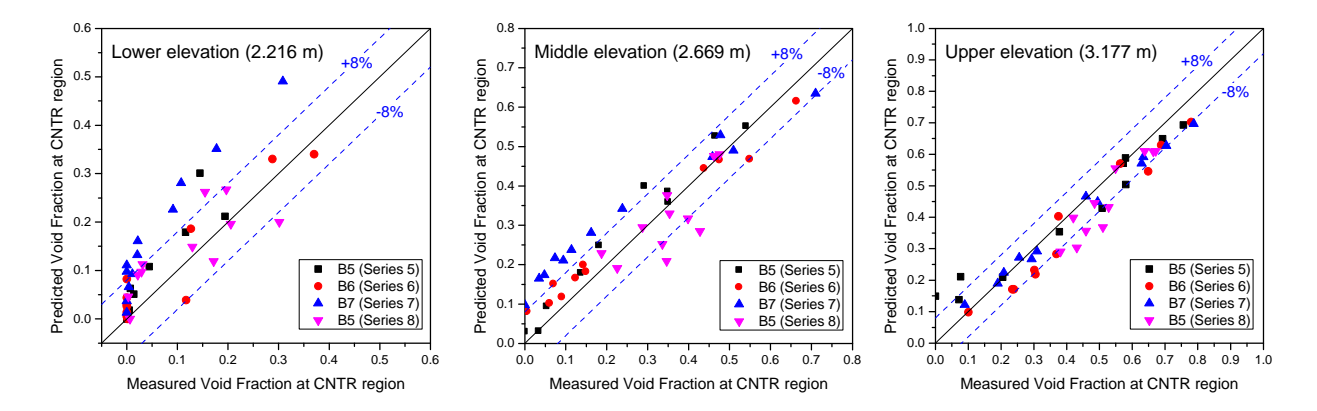


Figure 3 Prediction of subchannel void fraction at various axial elevations

2.3 Transient bundle void distribution benchmark

Transient bundle void distribution benchmark provided subchannel averaged void fraction at the 3 different axial levels of CNTR region under four transient conditions: power increase (PI), flow reduction (FR), depressurization (DP), and temperature rise (TI). These data are important for the benchmark of the subchannel analysis codes in terms of predicting CHF for reactor transient or accident conditions. The homogeneous equilibrium model employed in the MATRA code revealed the maximum deviation between the predicted and measured values of averaged void fraction for the four different transients of PI, FR, DP, and TI as 0.247, 0.216, 0.209, and 0.285, respectively. For the flow reduction transient, the maximum and minimum errors of (P-M) were calculated by 0.076/-0.126 for B5 and 0.216/-0.077 for B7, respectively. The maximum deviation was found at the lower elevation of of B7 bundle as shown in Figure 4. The implicit scheme employed in the MATRA code allowed no restrictions in the time step size for the transient calculations.

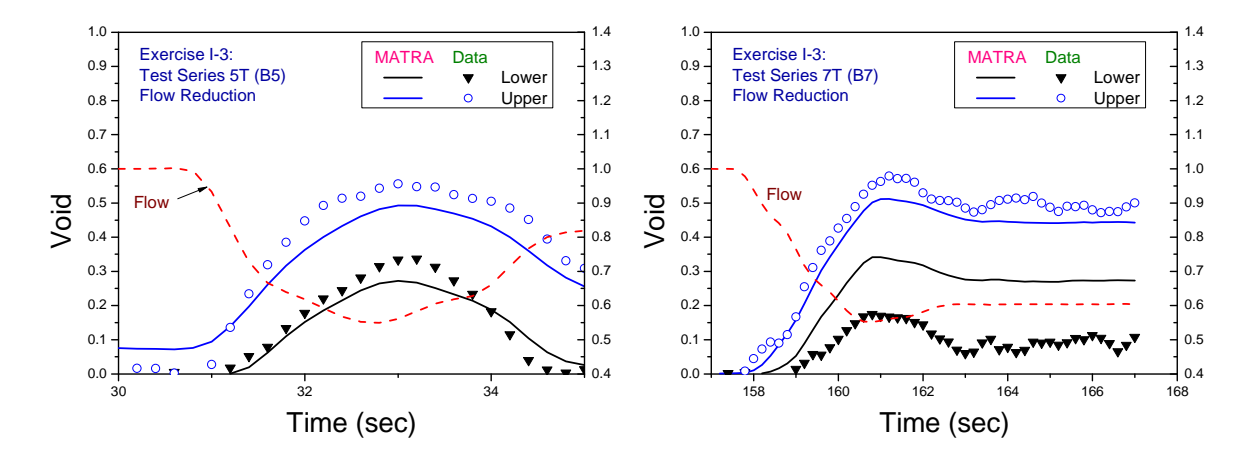


Figure 4 Subchannel void fraction under flow reduction transients

3. Analysis of Phase-II Benchmark Problems

3.1 Subchannel exit temperature distribution benchmark

The accuracy of a subchannel analysis code is fairly dependent on the modeling of interchannel exchanges between adjacent subchannels such as diversion cross flow and turbulent mixing [4]. The diversion cross flow caused by lateral pressure difference between subchannels is calculate from the eqs. $(1) \sim (4)$ which includes the lateral momentum equation. The turbulent mixing term is considered in the subchannel equations by eq. (5) which implies a turbulent mixing parameter defined as

$$\beta = \frac{\varepsilon_{ij}}{z_{ii}} \times \frac{\rho}{G} = \frac{v'_{ij}}{G/\rho}.$$
 (7)

where ε_{ij} , z_{ij} , and v'_{ij} are the mean turbulent eddy diffusivity of the heat, the mixing distance, and fluctuating velocity between sub-channels i and j, respectively. Subchannel exit temperatures were measured at the exit of a 5x5 mixing test bundle (A1) which has a large gradient of radial power distribution. The average power in the hot region is 4 times higher than that in the cold region. The prediction of subchannel temperature distribution is largely affected by the turbulent cross flow which is proportional to the magnitude of β . The optimum value of β is determined at the condition when the difference between measured and predicted values of region averaged exit temperature becomes minimum for various values of β .

The optimum values of β for various operating conditions were summarized in Table 3, and the mean value was calculated by 0.08. In the experimental results, there is the temperature gradient not only between hot (HH and HC) and cold region (CC and CH) but also between each region, which means that the temperature gradient exists between HH - HC region, and between CC - CH region

as shown in Figure 5. However, the temperature gradient between each cold and hot region does not appear in the predicted distribution. Thus, a higher value of β is resulted in the predicted distribution.

Case	P (MPa)	G (kg/m ² s)	T _{in} (°C)	Measured exit temperature (°C)				TDC
				НН	НС	СН	CC	
01-1237	4.9	4722	86.0	174.6	170.0	155.8	147.7	0.072
01-5125	14.7	3038	289.2	330.3	327.5	322.7	319.3	0.081
01-5215	14.7	3041	282.9	335.6	334.5	328.0	322.4	0.084
01-5237	14.7	4708	229.4	299.6	294.6	287.8	280.7	0.089
01-5252	14.7	541	113.9	194.6	194.2	175.9	172.4	0.053
01-5342	14.7	533	164.5	260.1	256.9	244.7	239.8	0.080
01-5343	14.7	1397	165.3	257.9	252.9	242.4	235.5	0.093
01-6232	16.6	583	251.5	315.3	312.1	304.8	300.9	0.083
01-6233	16.6	1361	254.0	322.7	318.2	311.5	305.1	0.089

Table 3 Optimum value of TDC at various operating conditions

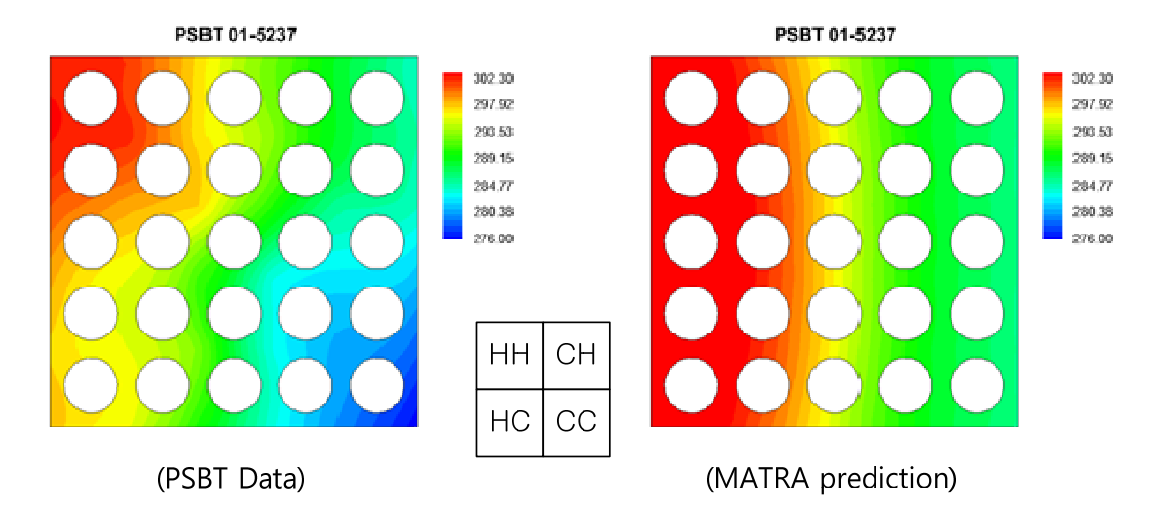


Figure 5 Comparison of fluid temperature distribution in a 5x5 test bundle.

A numerical analysis using CFD code(ANSYS, version 12.1) was conducted to investigate the influence of spacer grids on the subchannel temperature gradient in the test bundle A1. A simplified grid model was adopted for the analysis which focused on the effect of mixing vanes. The geometry of mixing vanes were properly considered as shown in Fig. 6-(a) due to their remarkable effects on the flow distribution. The computational meshes for the upper and lower parts of the mixing vanes were generated by applying the hexagonal sweep method while tetrahedron meshes were applied to the mixing vane region. The standard k-ε turbulence model and the convergence criterion of 10⁻⁶ RMS residual were used for the analysis of flow characteristics. An operating condition which was employed in Fig. 5 (i.e., 01-5237) was selected for this CFD analysis.

Figure 6-(b) shows the surface streamline at the location of 40 mm downstream of the mixing vane. As the result of CFD calculations, the fluid passing through the mixing vane forms a diagonal flow

as shown in Fig. 6-(b). This flow pattern induces vigorous mixing between HC and CH region which may result in the pattern of temperature gradient of PSBT data as shown in Fig. 5.

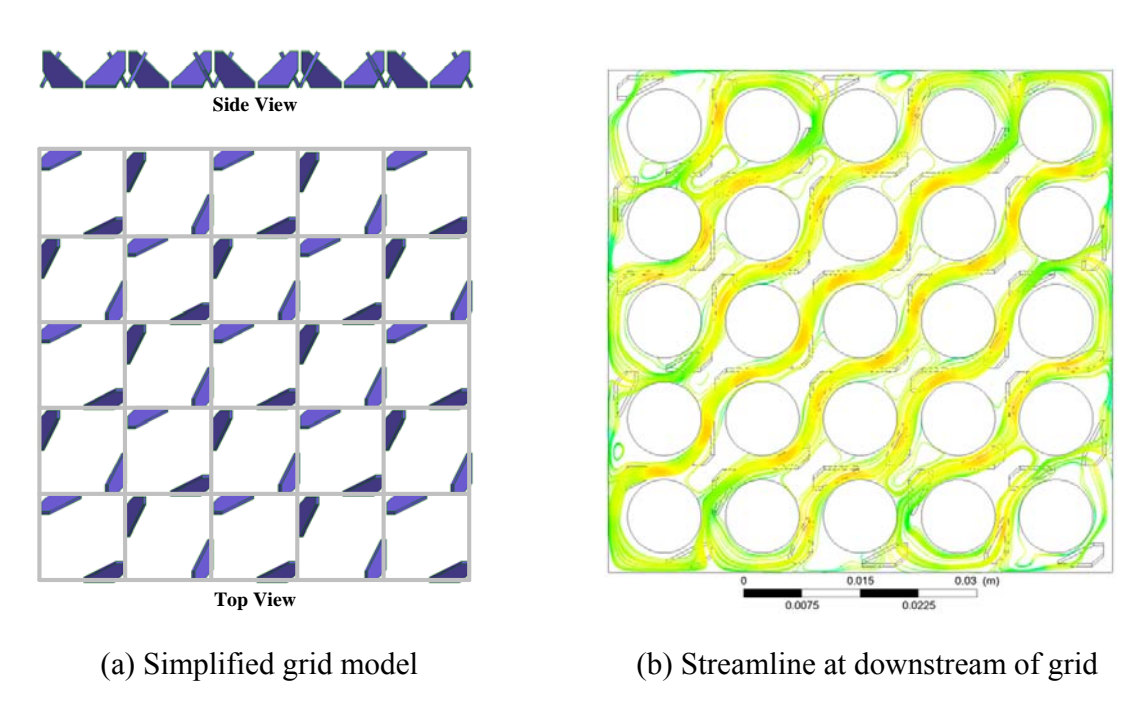


Figure 6 Modelling and results of CFD analysis.

3.2 Steady-state DNB benchmark

The steady-state DNB benchmark data provided the power at which DNB occurred and the corresponding location in the bundle. Various DNB prediction models including empirical correlations and mechanistic models, were evaluated for the benchmark data by employing subchannel-grade local thermal hydraulic conditions calculated by a subchannel code MATRA.

The EPRI correlation [5] is a generalized bundle correlation that has been developed on the basis of the local fluid conditions obtained with the COBRA-IIIC code and covering PWR and BWR normal operating conditions as well as hypothetical LOCA conditions. A CHF lookup table method [6] provides CHF values for water-cooled tubes at discrete values of pressure, mass velocity, and critical quality. Linear interpolation between table values gives the CHF for a specific condition, and several correction factors were introduced to extent the CHF table to various shapes of the boiling channel. The applicability of the CHF lookup table method with a subchannel analysis code has been assessed for CHF data for square-latticed rod bundles [7]. Two mechanistic models for DNB were selected: a sublayer dryout model and a bubble crowding model. The sublayer dryout model is developed on the basis of the dryout of a thin liquid sublayer underneath a vapor blanket flowing over the heated wall. Key parameters associated with this model are sublayer thickness, blanket velocity and blanket geometry. The mean length of vapor blanket is governed by the hydrodynamic instability of the vapor-liquid interface, and the blanket diameter is calculated by an

appropriate correlation. Lin and his coworkers [8] suggested a physical model based on the assumption that the velocity of the vapor blanket should be the superposition of the local liquid velocity and the relative vapor blanket velocity which can be determined by a balance between the buoyancy and drag forces exerted on the blanket. They examined the model for selected rod bundle data with COBRA-IIIC/MIT-1 code. The near-wall bubble crowding model postulated that CHF at low qualities occurs when the bubbles near the heated wall coalesce into a vapor film. The bubble layer near the wall was assumed to become so thick that it inhibits enthalpy transport between the fluid in the core region and the liquid near the wall. Weisman and his coworkers suggested that CHF occurs when the void fraction in the bubbly layer just exceeds the critical value of 0.82. During the modeling of turbulent interchange between the bubbly layer and core regions, two empirically determined parameters have been adopted. Weisman and Ying [9] suggested an extended version of the bubble crowding model to high quality and low velocity conditions. They evaluated the model for rod bundle data under PWR conditions using COBRA-IV-I code.

The CHF values predicted by the four different DNB prediction models were compared with the measured data as shown in Fig. 7, and the P/M statistics were summarized in Table 4. For the test bundles with uniform and cosine axial power shape, the mean error of (P/M) for EPRI correlation and the AECL-IPPE 1995 CHF lookup table were calculated by -2.7% and -3.0%, respectively. The sublayer dryout model under-predicted the CHF data about 4.9% while the bubble crowding model over-predicted about 16.4% as shown in Table 4.

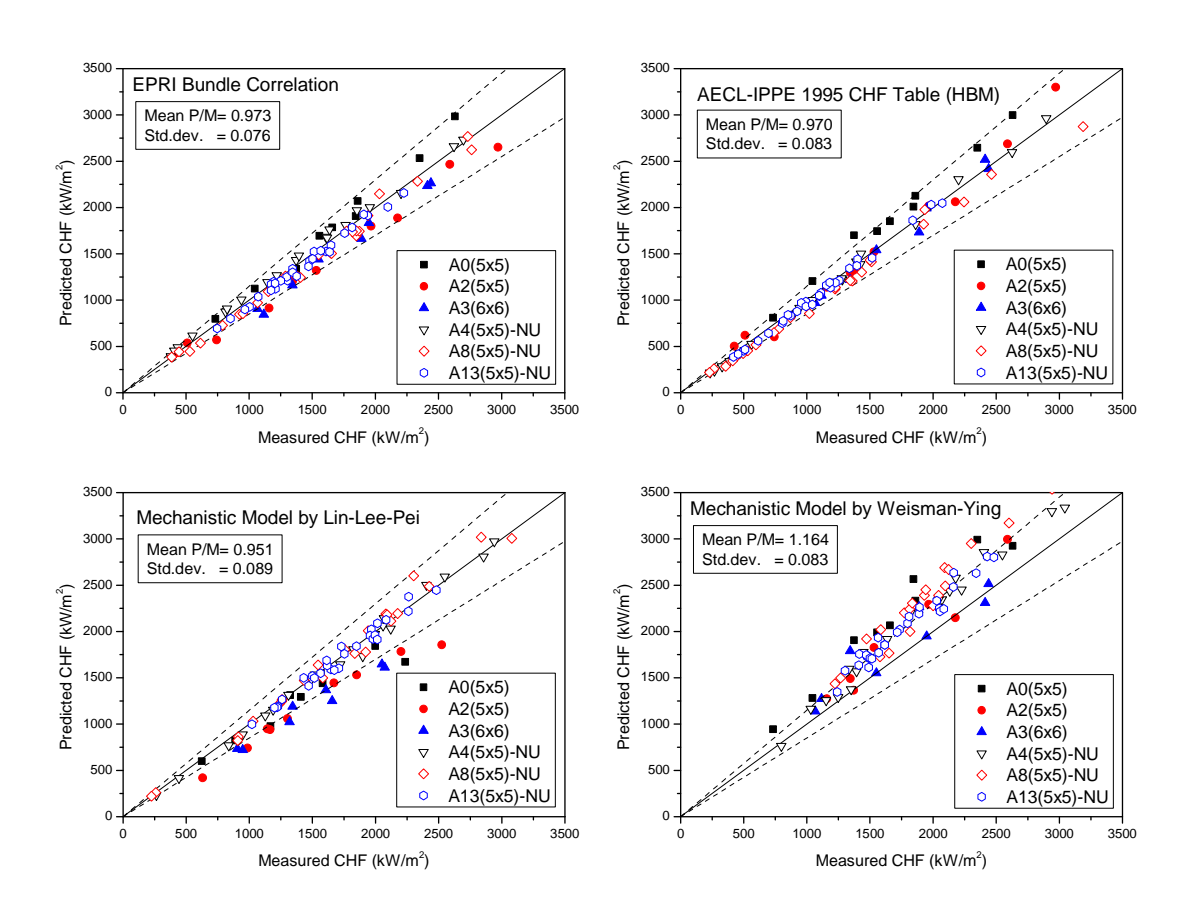


Figure 7 Evaluation of various CHF prediction models for steady-state CHF in test bundles

Series		Bundle correlation	Tube correlation Mechanistic mo		stic model
		EPRI [5]	AECL-1995 [6]	Lin-Lee-Pei [8]	Weisman-Ying [9]
A0	AVG/STD	1.073/0.046	1.136/0.042	0.911/0.077	1.272/0.084
A2	AVG/STD	0.903/0.084	1.021/0.113	0.790/0.061	1.137/0.069
A3	AVG/STD	0.885/0.062	0.966/0.054	0.802/0.046	1.091/0.126
A4	AVG/STD	1.054/0.038	0.957/0.054	0.976/0.043	1.125/0.068
A8	AVG/STD	0.945/0.049	0.906/0.051	1.003/0.049	1.207/0.067
A13	AVG/STD	0.961/0.028	0.964/0.037	0.996/0.033	1.152/0.044
Total	AVG/STD	0.973/0.076	0.970/0.083	0.951/0.089	1.164/0.083

Table 4 P/M statistics for DNB test bundles with uniform APS

4. Conclusion

A subchannel code MATRA was employed for evaluation of void distribution benchmark and DNB benchmark. For the steady-state subchannel void distribution in test bundles, the mean error and standard deviation were calculated by 1.4% and 7.3%, respectively. MATRA code tended to overpredict the void fraction at the central region at lower elevation, and the maximum mean error was calculated by 11.0% for the test bundle with cosine axial power shape. Similarly, for transient void benchmark, relatively large prediction error was observed at lower elevations.

For the fluid temperature benchmark data, the best estimated value of the turbulent mixing parameter was calculated as 0.08 with a standard deviation of 0.011. As the result of a CFD analysis, the temperature gradients inside the hot and cold regions were possibly explained by the mixing vane effect.

DNB data for test bundles with uniform and cosine axial power shape was evaluated by employing various CHF prediction models. Two different mechanistic DNB models were selected for this benchmark: a sublayer dryout model and a near wall bubble crowding model. The mean error and standard deviation of P/M were calculated by $-4.9\% \sim +16.4\%$ and $8.3\% \sim 8.9\%$, respectively. The AECL-IPPE 1995 CHF lookup table by employing a heat balance method and EPRI correlation revealed the mean error as -3.0% and -2.7%, respectively.

5. References

- [1] A. Rubin, et. al., "OECD/NRC Benchmark Based on NUPEC PWR Subchannel and Bundle Tests (PSBT) Volume I: Experimental Database and Final Problem Specifications," NEA/NSC/DOC(2010)1, Nov. (2010).
- [2] S.G. Beus, A two-phase turbulent mixing model for flow in rod bundles, Westinghouse Report, Bettis Atomic Power Laboratory, WAPD-T-2438 (1971).
- [3] D.H. Hwang, Y.J. Yoo, W.K. In, and S.Q. Zee, "Assessment of the Interchannel Mixing Model with a Subchannel Analysis Code for BWR and PWR Conditions," *Nuclear Engineering Design*, Vol. 199, 2000, pp. 257-272.

The 14th International Topical Meeting on Nuclear Reactor Thermalhydraulics, NURETH-14 Toronto, Ontario, Canada, September 25-30, 2011

- [4] Rogers, J.T., R.G. Rosehart, 1972. "Mixing by turbulent interchange in fuel bundles: Correlations and inferences," ASME, 72-HT-53.
- [5] D.G. Reddy and C.F. Fighetti, "Parametric Study of CHF Data Volume 2. A generalized subchannel CHF correlation for PWR and BWR fuel assemblies," EPRI-NP-2609, (1983).
- [6] D.C. Groeneveld, et. al., "The 1995 look-up table for critical heat flux in tubes," *Nuclear Engineering Design*, Vol. 163, 1996, pp. 1-23.
- [7] D.H. Hwang, et. al., "A comprehensive assessment of round tube CHF prediction models for square-latticed rod bundles," *Proc. 20th International heat transfer Conf.*, 4, pp.309-314., Grenoble, 2002 Aug. 18-23.
- [8] W.S. Lin, et. al., "A theoretical critical heat flux model for rod bundles under pressurized water reactor conditions," *Heat Transfer and Fluid Flow*, Vol. 88, 1989, pp. 213-226.
- [9] J. Weisman and S.H. Ying, "A theoretically based critical heat flux prediction for rod bundles at PWR conditions," *Nuclear and Engineering and Design*, Vol. 85, 1985, pp. 239-250.